American Journal of Pathology, Vol. 168, No. 2, February 2006

DOI: 10.2353/ajpath.2006.050312

Gastrointestinal, Hepatobiliary and Pancreatic Pathology

Consequences of Copper Accumulation in the Livers of the *Atp7b*$^{-/-}$ (Wilson Disease Gene) Knockout Mice

Dominik Huster,* Milton J. Finegold,† Clinton T. Morgan,* Jason L. Burkhead,* Randal Nixon,‡ Scott M. Vanderwerf,* Conrad T. Gilliam,§ and Svetlana Lutsenko*

From the Departments of Biochemistry and Molecular Biology and Pathology,‡ Oregon Health & Science University, Portland Oregon; the Department of Pathology,† Texas Children's Hospital, Houston, Texas; and the Department of Genetics and Development,§ Columbia University, New York, New York*

Wilson disease is a severe genetic disorder associated with intracellular copper overload. The affected gene, *ATP7B*, has been identified, but the molecular events leading to Wilson disease remain poorly understood. Here, we demonstrate that genetically engineered *Atp7b*$^{-/-}$ mice represent a valuable model for dissecting the disease mechanisms. These mice, like Wilson disease patients, have intracellular copper accumulation, low-serum oxidase activity, and increased copper excretion in urine. Their liver pathology developed in stages and was determined by the time of exposure to elevated copper rather than copper concentration per se. The disease progressed from mild necrosis and inflammation to extreme hepatocellular injury, nodular regeneration, and bile duct proliferation. Remarkably, all animals older than 9 months showed regeneration of large portions of the liver accompanied by the localized occurrence of cholangiocarcinoma arising from the proliferating bile ducts. The biochemical characterization of *Atp7b*$^{-/-}$ livers revealed copper accumulation in several cell compartments, particularly in the cytosol and nuclei. The increase in nuclear copper is accompanied by marked enlargement of the nuclei and enhanced DNA synthesis, with these changes occurring before pathology development. Our results suggest that the early effects of copper on cell genetic material contribute significantly to pathology associated with *Atp7b* inactivation. ***(Am J Pathol 2006, 168:423–434; DOI: 10.2353/ajpath.2006.050312)***

Copper is an essential co-factor of key metabolic enzymes that participate in a variety of physiological processes, including respiration, neurotransmitter biosynthesis, radical detoxification, and iron uptake.[1,2] However, excess copper must be promptly exported from the cell because accumulated metal disrupts normal cell homeostasis, causing protein malfunction, lipid peroxidation, and DNA mutations.[3,4] In humans, mutations in *ATP7B*, which encodes the copper-transporting P-type ATPase, are associated with marked accumulation of copper in tissues and with a wide spectrum of pathological changes, manifesting as Wilson disease (WD).

Understanding and treating WD is challenging. WD patients may suffer from liver disease, neurological or psychiatric abnormalities, or various combinations of these symptoms.[5,6] Despite identification of more than 200 causative mutations, no strong genotype-phenotype correlations in WD have been found.[7] The hepatic course of WD is diverse, ranging from self-limited hepatitis and chronic active hepatitis to cirrhosis and fulminant hepatic failure.[6] No specific biochemical or genetic markers firmly predict the severity of the disease or response to treatment. Therefore, there is a great need for better understanding of the molecular basis of WD and for reliable models of copper-induced toxicity.

Several inbred rodent strains are available to study the consequences of copper overload in the liver. The toxic milk (*tx*) mouse and the Jackson *tx* mouse (*tx*^{j}) have missense mutations in *Atp7b* that do not disrupt Atp7b synthesis but affect Atp7b function.[8–11] The Long-Evans Cinnamon rat (LEC rat) has a 300-bp deletion in *Atp7b*, resulting in the loss of protein.[12] All these animals accumulate copper in the liver and show a wide spectrum of liver pathologies ranging from nodular but otherwise phenotypically normal liver in the *tx* mice to massive necrosis, fulminant hepatitis, and hepatocellular carcinoma in LEC

Supported by the National Institutes of Health (grant 1 P01 GM 067166-01 to S.L.) and the Deutsche Forschungsgemeinschaft (postdoctoral fellowship HU 932/1-1 to D.H.).

Accepted for publication October 20, 2005.

Address reprint requests to Svetlana Lutsenko, OHSU, L224, Sam Jackson Park Rd., Portland, OR 97239. E-mail: lutsenko@ohsu.edu.

rat livers.[13–15] These variations could be due to species-specific hepatic response to copper overload; however, incomplete inactivation of Atp7b (in the *tx* mice) and/or the involvement of other genes mutated in the inbred animals cannot be excluded. (For example, LEC rats of different lineage show markedly different propensity for development of hepatocellular carcinoma; the reason for this phenotypic variation is not clear and could be due to additional mutations in one of the lineages[14].) Consequently, to better understand the effects of copper on liver metabolism and to link directly inactivation of Atp7b to specific liver abnormalities, we used genetically engineered *Atp7b*$^{-/-}$ mice, a new model developed for analysis of WD.[16] The initial advantages of these animals compared to the other models include a well-defined genetic background and the availability of the original strain to serve as a control in comparative analyses. Here, we demonstrate that *Atp7b*$^{-/-}$ mice also have biochemical characteristics resembling WD patients and display distinct and remarkable liver pathology. We conclude that these animals represent an excellent model for analysis of hepatic copper toxicity.

Materials and Methods

Mice

The generation of the *Atp7b*$^{-/-}$ mice has been described previously.[16] Mice were maintained on strain C57BLx129S6/SvEv and housed at the Oregon Health and Science University Department of Comparative Medicine according to the National Institutes of Health guidelines on the use of laboratory and experimental animals; animals of both sexes were used. Food and water were provided *ad libitum* and no further treatment was performed. Mice were fed with Rodent Diet 5001 (Lab Diet, St. Louis, MO), containing 13 ppm Cu, 70 ppm Zn, and 270 ppm Fe. Animals were euthanized at given time points; livers were quickly removed, immediately frozen in liquid nitrogen, and stored at −80°C. Blood was collected by cardiac puncture and serum was separated by centrifugation after blood coagulation and stored at −80°C until further use.

Copper Measurements

Pieces of liver (50 to 100 mg) were homogenized in 500 μl of 0.1 mol/L sodium phosphate buffer (pH 7.5), 0.25 mol/L sucrose (buffer A) in a loose-fitting Dounce homogenizer. The copper content was then determined by atomic absorption spectrometry using an AA-6650 atomic absorption spectrophotometer (Shimadzu Corp., Kyoto, Japan). Copper levels were normalized to the amount of protein in the homogenate, which was determined by the method of Lowry and colleagues.[17] Serum copper concentration was measured directly by atomic absorption spectrometry after dilution of the serum in water. To determine daily urinary copper excretion, the control and *Atp7b*$^{-/-}$ mice were placed into metabolic cages, urine was collected throughout 24 hours, and the copper content was measured by atomic absorption spectrometry and corrected for volume. To measure the distribution of copper between cytosol and membrane compartments, the homogenate was centrifuged for 5 minutes at 500 × *g* to remove crude cell debris and then at 125,000 × *g* for 30 minutes. The supernatant was separated from the pellet, the pellet was resuspended in buffer A, and copper was measured by atomic absorption spectrometry in both fractions.

The distribution of copper in a soluble fraction was further analyzed by gel-filtration. The fraction was separated on a Tricorn Superose 12 10/300 GL column (Amersham Biosciences, Arlington heights, IL) equilibrated with 0.05 mol/L phosphate buffer, 0.15 mol/L NaCl, pH 7.0. Molecular weight standards (Sigma Chemical Co., St. Louis, MO) including dextran (MW 2000 kd), bovine serum albumin (MW 66 kd), trypsin Inhibitor (MW 20 kd), cytochrome *c* (MW 12 kd), and aprotinin (MW 6.5 kd) were used for calibration. Fractions (500 μl) were collected; aliquots from each fraction were diluted 1:10 with distilled water, and copper concentration was determined by atomic absorption spectrometry.

To examine distribution of copper in subcellular compartments, membranes were fractionated using a modified method of Fleischer and Kervina.[18] Briefly, liver homogenates were centrifuged in several steps (10 minutes at 500 × *g*, nuclei-enriched fraction; 15 minutes at 3000 × *g*, mitochondria-enriched fraction; 20 minutes at 15,000 × *g*, ER/Golgi-enriched fraction; and 30 minutes at 125,000 × *g*, plasma membrane-enriched fraction). The pellets were resuspended in 100 μl of water and copper content was determined as described above.

Purification and Characterization of Nuclear Fraction

Nuclei were isolated from frozen liver tissue using a sucrose step gradient as described[19] with the following modifications. Tissue (300 mg) was homogenized in 0.8 ml of homogenization buffer [0.25 mol/L sucrose, 20 mmol/L HEPES, pH 7.5, 1 mmol/L $MgCl_2$, and Complete protease inhibitors (Roche, Indianapolis, IN)] in a Dounce glass tissue homogenizer using eight strokes with a loose pestle and then 10 strokes with the tight pestle. The homogenate was centrifuged at 4°C for 10 minutes at 1000 × *g*. The supernatant was kept as postnuclear supernatant and the pellet was resuspended in 1 ml of 1.6 mol/L sucrose and the same buffer as above. Resuspended material was layered on top of 2.2 mol/L sucrose in the homogenization buffer, overlayed with homogenization buffer, and centrifuged at 75,000 × *g* for 45 minutes. The pellet from the 2.2 mol/L step contained purified nuclei, while mitochondria were retained at the 2.2 mol/L/1.6 mol/L interface.

To confirm purity of nuclei, 20 μg of fractions from the sucrose step gradient were separated by 12% sodium dodecyl sulfate-polyacrylamide gel electrophoresis and transferred to polyvinylidene difluoride for immunodetection. Mouse monoclonal anti-Na/K ATPase α1 (Affinity Bioreagents, Golden, CO) was used to detect plasma

membrane fraction; rabbit anti-cytochrome *c* α subunit antibody was a kind gift from Dr. James Hare (Oregon Health and Science University) and was used to identify the presence of mitochondria. The rabbit anti-histone H2B antibody was a kind gift from Dr. Hua Lu (Oregon Health and Science University) and was used to indicate presence of nuclear proteins. The staining was visualized using secondary antibodies, coupled to fluorophore (anti-mouse IgG-Alexa Fluor 680; Molecular Probes, Eugene, OR; donkey anti-rabbit IgG-IRDye 800; Rockland, Rockford, IL), and an Odyssey Scanner (LiCor, Lincoln, NE). All incubations with antibody were at 1:10,000 dilution in SuperBlock T20 (Pierce, Rockford, IL).

Analysis of Alanine Aminotransfersase (ALT) and Ceruloplasmin

The activity of serum ALT was determined by automated measurement (ANTECH-Diagnostics, Portland, OR). For analysis of ceruloplasmin, 1 μl of serum was treated before sodium dodecyl sulfate-polyacrylamide gel electrophoresis, either under reducing/denaturing conditions (3.3% sodium dodecyl sulfate, 2.7% urea, 5% β-mercaptoethanol, 62.5 mmol/L Tris, pH 6.8) to determine the total amount of ceruloplasmin or nonreducing/nondenaturing conditions (1% sodium dodecyl sulfate, 10% glycerol, 62.5 mmol/L Tris, pH 6.8) to separate the apo- and copper-bound forms of ceruloplasmin. Proteins were transferred to Immobilon-P (Millipore, Bedford, MA) and ceruloplasmin was detected using goat anti-human-ceruloplasmin antibody (Sigma). Ceruloplasmin activity was evaluated by measuring the oxidase activity in serum using two different protocols[20,21] that produced consistent results. The data shown in Figure 1C were generated using the method from Schosinsky and colleagues.[21]

RNA Isolation for Microarrays

Total RNA was isolated from control and *Atp7b*$^{-/-}$ mouse livers (three of each) using Trizol reagent (Invitrogen, Carlsbad, CA) according to the manufacturer's recommendations and purified using an RNeasy cleanup procedure (RNeasy mini kit; Qiagen, Valencia, CA). The integrity of isolated RNA was electrophoretically verified by ethidium bromide staining and by optical density (OD) absorption ratio ($OD_{260\ nm/280\ nm}$, >1.8). The RNA was used for hybridization to the GeneChip Mouse Genome 430A Array (Affymetrix, Santa Clara, CA) at the Oregon Health and Science University Microarray Core Facilities. Analysis of data performed at the Microarray Core Facilities revealed no change in the *Atp7a*-related signal.

Histology and Immunohistochemistry

The tissue sections were prepared by fixing livers in 10% buffered formalin at pH 7.4 for 48 to 72 hours, transferring to 80% ethanol, and then embedding in paraffin. The sections were stained with hematoxylin and eosin (H&E), periodic acid-Schiff with and without previous diastase

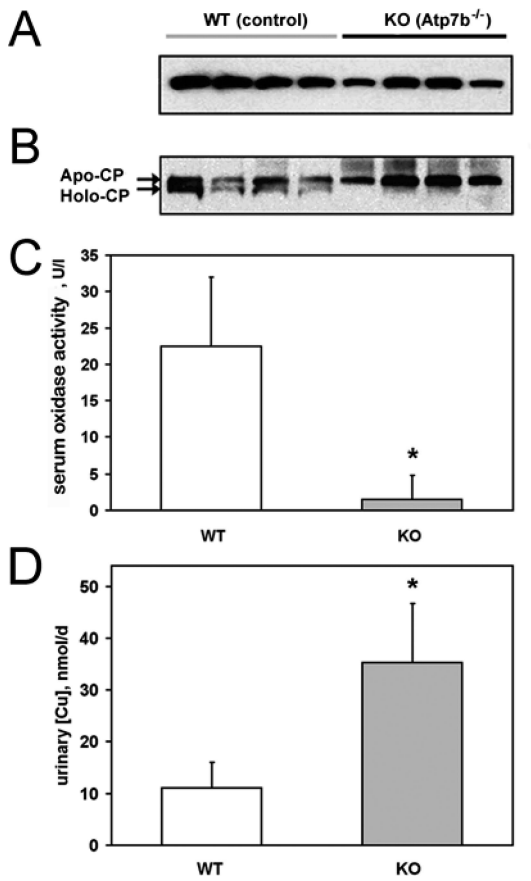

Figure 1. Copper incorporation into ceruloplasmin is disrupted by *Atp7b* inactivation. **A:** Total amount of ceruloplasmin in the serum analyzed under reducing and denaturing conditions. **B:** Detection of holo- and apo-ceruloplasmin in the same samples after separation under nonreducing, nondenaturing conditions. In both cases, the equal amounts of total serum protein from four different 6-week-old WT and KO mice were analyzed. **C:** Oxidase activity in serum of 6-week-old WT and KO mice. **D:** Daily urinary copper excretion in 6-week-old WT and KO mice ($n = 5$ to 7; *statistical significance for KO versus WT mice, $P < 0.01$).

treatment, and rhodamine for copper. DNA synthesis was evaluated with Mib-1 antibody to Ki67 (Novocastra, Newcastle, UK) after antigen retrieval with ethylenediaminetetraacetic acid. Antibody dilution was 1:1000. α-Fetoprotein was detected after microwave heating with anti-mouse antibody (ICN, Irvine, CA); using a dilution of 1:3000. Antibody to mouse cytokeratin 19 was kindly provided by Professor Lucie Germain (Laval University, Quebec, Canada) and used after ethylenediaminetetraacetic acid antigen retrieval. Dilution was 1:20. Apoptosis was evaluated by the terminal dUTP nick-end labeling *in situ* assay following the manufacturer's protocol after proteinase K digestion (Serologics Corp., Norcross, GA).

Electron Microscopy

Portions of liver were immersed in 3% glutaraldehyde in 0.1 mol/L phosphate buffer, pH 7.4. After overnight fixation they were transferred to 0.1 mol/L phosphate buffer and then postfixed in 1% OsO_4 for 2 hours. The tissue was dehydrated in ethanol, rinsed in propylene oxide, and embedded in Epon. Sections (400 μm) were cut on

Table 1. Age-Dependent Changes in Copper Concentration in the Liver and Serum of the Control *Atp7b*$^{+/+}$ (WT) and *Atp7b*$^{-/-}$ (KO) Mice

Age (weeks)	Liver copper (ng/mg protein)		Liver copper ratio (KO/WT)	Serum copper (ng/ml)		Serum copper ratio (KO/WT)
	Atp7b$^{+/+}$	*Atp7b*$^{-/-}$		*Atp7b*$^{+/+}$	*Atp7b*$^{-/-}$	
6	82.3 ± 37.4	1496.3 ± 220.5*	18.2	480.6 ± 47.8	412.3 ± 195.4	0.9
20	37.2 ± 16.6	1372.7 ± 385.3*	36.9	728.2 ± 208.4*	1648.8 ± 337.2	2.3
28	34.2 ± 17.4	627.2 ± 85.9*	18.4	497.4 ± 229.7*	1171.7 ± 183.8	2.4
36	39.4 ± 15.2	489.6 ± 100.0*	12.4	503.6 ± 102.3*	1179.9 ± 485.8	2.3
44	36.8 ± 12.9	573.9 ± 55.9*	15.6	400.8 ± 183.8*	1147.9 ± 501.8	2.9

$n = 3$ to 7.
*Statistical significance for KO versus WT animals at the same age, $P < 0.05$.

a Reichert ultramicrotome, stained with uranyl acetate, and viewed and photographed in a JOEL 100CX transmission electron microscope.

Results

Age-Dependent Changes in Copper Concentrations in the Liver and Serum of *Atp7b*$^{-/-}$ Mice

Hepatic copper accumulation is a diagnostic feature of WD. Analysis of copper concentration in the livers from 24 *Atp7b*$^{-/-}$ (knockout, KO) and 27 wild-type (WT) mice confirmed a statistically significant difference between KO and WT animals at all ages (Table 1), in agreement with our initial report.[16] The highest level of copper was detected at 5 to 6 weeks of age and did not change significantly for the next 4 months. However, the excess of copper compared to the control (the KO:WT ratio) did increase from ~18-fold at 5 to 6 weeks to ~37-fold in 20-week-old mice due to decrease of copper in the WT animals. Subsequently, the copper levels decreased in both KO and WT animals by ~50%, but the difference between the control and KO samples remained high (~12- to 18-fold) and statistically significant (Table 1).

A different trend was observed in the serum (Table 1). At 5 to 6 weeks when concentration of copper in the liver was already high, the serum copper remained similar to the control levels. In the older KO animals, serum copper peaked at 20 weeks and remained elevated (~2.3- to 2.9-fold), whereas in the WT mice it stayed unchanged. There was no change in the serum copper concentration in KO animals from 28 to 44 weeks of age.

The Generation of Holo-Ceruloplasmin Is Disrupted in the *Atp7b*$^{-/-}$ Mice

Along with copper accumulation, another expected consequence of Atp7b inactivation markedly decreased copper incorporation into ceruloplasmin, a secreted copper-dependent ferroxidase produced in the liver. In the vast majority of WD patients, ceruloplasmin levels in the plasma are reduced because of rapid elimination of apoprotein,[5] although levels of ceruloplasmin close to normal were also reported.[22] In the serum of *Atp7b*$^{-/-}$ mice, the total amount of ceruloplasmin did not show marked changes; it was reduced in some animals, but was comparable to the WT levels in others (Figure 1A). However, when the same *Atp7b*$^{-/-}$ samples were analyzed under nonreducing, nondenaturing conditions, which permit separation of holo- and apo-ceruloplasmin,[23] it became apparent that all samples of *Atp7b*$^{-/-}$ serum contained only apo-ceruloplasmin, whereas both apo- and holo-ceruloplasmin were detected in the WT serum (Figure 1B).

To further confirm that Atp7b inactivation results in production of apo-ceruloplasmin, which is catalytically inactive, we measured oxidase activity in serum samples from control and KO animals. Marked decrease of ceruloplasmin-mediated oxidase activity in serum is a diagnostic feature of WD; similarly to WD patients, the oxidase activity in the serum of the *Atp7b*$^{-/-}$ mice was markedly reduced (Figure 1C) in full agreement with the observed absence of holo-ceruloplasmin.

The lack of copper incorporation into ceruloplasmin has further important consequences. Normally, copper bound to ceruloplasmin constitutes vast majority (95%) of total serum copper. When holo-ceruloplasmin is absent, copper apparently binds to low-molecular weight molecules, which can be filtered by kidney and excreted into urine. In fact, markedly elevated levels of copper in the urine represent one of the most reliable biochemical indicators of WD in humans. Measurements of copper content in the urine of *Atp7b*$^{-/-}$ mice revealed that in these animals urinary copper was highly elevated (Figure 1D), reflecting increased amounts of copper, which can be filtered. Thus, the major biochemical characteristics of WD, such as intracellular copper accumulation, disrupted copper incorporation into ceruloplasmin, low oxidase activity in serum, and elevated levels of copper in urine, were clearly observed in *Atp7b*$^{-/-}$ mice.

Copper-Induced Changes in Liver Morphology

Comparison of control and *Atp7b*$^{-/-}$ livers revealed marked consequences of copper accumulation for liver morphology. The magnitude of the effect correlated with the length of exposure to elevated copper rather than actual copper concentration in the liver. At 6 weeks, when copper concentration is at its maximum level, the livers of *Atp7b*$^{-/-}$ animals appeared slightly smaller than in WT animals, but no obvious abnormalities in color or shape were detected. Beginning at ~20 weeks, the *Atp7b*$^{-/-}$

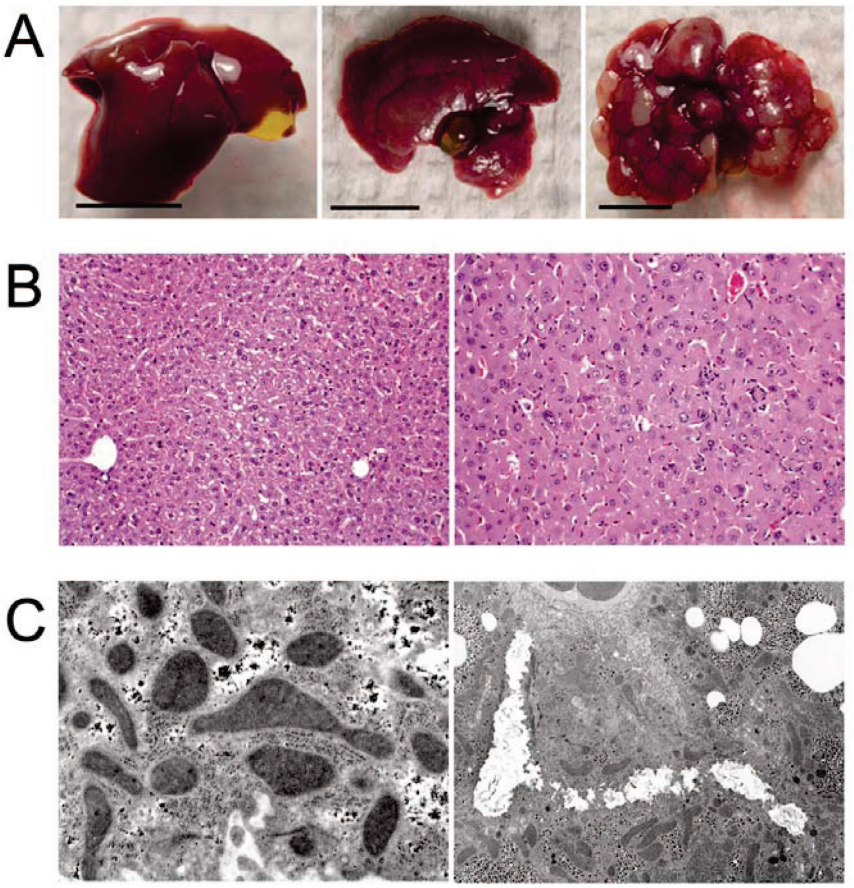

Figure 2. Macroscopic and microscopic changes in the *Atp7b*$^{-/-}$ livers. **A:** Control liver (**left**) and two *Atp7b*$^{-/-}$ livers (**middle** and **right**) illustrating different degrees of pathological changes at 20 weeks. **B:** H&E staining at 6 weeks. **Left**: Unremarkable histology. **Right**: Enlarged hepatocytes, containing pleomorphic nuclei, foci of single cell necrosis, and mild lobular inflammation. **C:** Electron microscopy of *Atp7b*$^{-/-}$ liver at 6 weeks. **Left**: Mitochondria have abnormal shape and size, as in human WD. **Right**: A dilated bile canaliculus and microsteatosis of a hepatocyte. Original magnifications: ×200 (**B**); ×10,000 (**C**, **left**); ×3000 (**C**, **right**).

livers became enlarged, with brown and gray nodules distinct from remaining normal parenchyma (Figure 2A). The extent of changes was comparable in animals of 20 and 28 weeks, and nodules were found in all KO mice at this age. After 36 weeks, the abnormalities were prominent in all KO animals.

Light Microscopy and Immunohistochemistry

Microscopic changes in the *Atp7b*$^{-/-}$ livers can be divided into three distinct phases depending on the age of animals. At the age of 5 to 6 weeks, the pathology was either absent or mild. In 50% of the 6-week-old mice (four of eight mice examined) the histology was completely unremarkable (Figure 2B, left). The other four mice had focal hepatocellular swelling, necrosis, and inflammation (Figure 2B, right). Glycogen stores were depleted in the latter group, and enlarged pleomorphic nuclei with prominent nucleoli were observed. Electron microscopy revealed focally distorted and enlarged mitochondria (Figure 2C, left) and focally dilated bile canaliculi (Figure 2C, right) even in the microscopically normal livers.

At the next stage (12 to 20 weeks and older), the pathology was much more extensive despite the lack of further increase in hepatic copper concentration. We observed uniformly severe hepatocellular injury with widespread necrosis and inflammation and remarkable nuclear enlargement with prominent nucleoli and vacuolization (Figure 3A). Copper was detectable in the cytoplasm of a small fraction of hepatocytes at this stage (not shown). Focal proliferation of bile ducts, including elongation and focal proliferation of small oval-like cells in the portal tract, was accompanied by acute cholangitis in 3 of 10 mice (Figure 3B). Fibrosis was found in 4 of 10 animals in relation to chronic inflammation in portal tracts around the bile ducts. Scattered macrophages, some forming multinucleated cells, and focal steatosis were also detected. Electron microscopy of the 12-week-old KO livers revealed striking enlargement of nuclei containing lipid droplets, pseudoinclusions, and very atypical fragmented nucleoli (Figure 3C), in half of the animals. These dysplastic changes were accompanied by abundant cytoplasmic accumulation of α-fetoprotein (Figure 3D).

Beginning at 28 weeks and continuing to 52 weeks, there was remarkable restoration of normal architecture of parenchyma and bile ducts in large portions of the liver (Figure 3, E and G). Neither copper nor α-fetoprotein was detectable and ultrastructural examination showed completely unremarkable hepatocytes (Figure 3H). However,

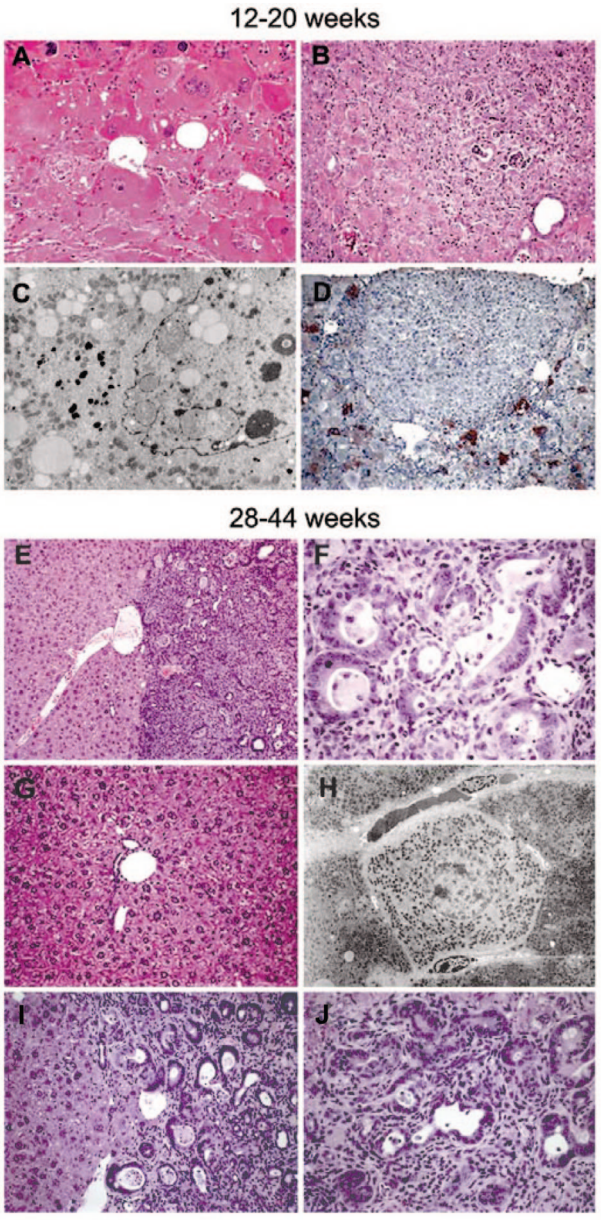

Figure 3. Extensive pathology, subsequent liver regeneration, and development of cholangiocarcinoma. **A:** Inflammation and necrosis of markedly enlarged hepatocytes with huge and deformed nuclei. **B:** Focal bile duct dilation and diffuse lobular chronic inflammation. **C:** Electron microscopy of a markedly enlarged nucleus with pseudoinclusions, lipid inclusions, and fragmented nucleoli. **D:** The dysplastic changes in hepatocytes are revealed by cytoplasmic accumulation of α-fetoprotein (brown). The central nodule of regenerating hepatocytes is unstained. **E:** Restoration of normal parenchyma (**left**) and tumor development (**right**). **F:** Focal extensive atypical proliferation of bile ducts and acute inflammation. **G:** Region of normal parenchyma contains an unremarkable portal tract with intact bile duct. **H:** Electron microscopy of a completely normal hepatocyte from the regenerating portions of the liver. **I** and **J:** Examples of marked complexity and irregularity of the tubular structures and significant pleomorphism of the epithelium, with the loss of usual basal nuclear polarity, anisonucleosis, and occasional mitoses. Original magnifications: ×200 (**A**, **D**, **G**, **I**); ×125 (**B**); ×2000 (**C**); ×100 (**E**); ×500 (**F**); ×1200 (**H**); ×360 (**J**).

in 4 of 14 mice beginning at 28 weeks of age and in all mice older than 36 weeks, there were multiple foci of extensive atypical proliferation of bile ducts, which was accompanied by intense acute inflammation and fibrosis (Figure 3, E and F). The number and complexity of ducts increased dramatically, even as the hepatic parenchyma was restored toward normal (Figure 3E). The inflammation becomes both acute and chronic and was associated with focal fibrosis in the expanded portal tracts. The ducts were lined by a single layer of enlarged columnar epithelial cells with hyperchromatic nuclei. Also, in several foci of each liver, we observed extremely distorted ducts lined by multiple layers of cells with high nuclear-cytoplasmic ratio, hyperchromasia, and dispolarity, consistent with displasia and probable carcinomatous transformation (Figure 3F).

More detailed examination of the duct lesion (Figure 3, I and J) showed marked complexity and irregularity of the tubular structures and significant pleomorphism of the epithelium, with the loss of usual basal nuclear polarity, anisonucleosis, and occasional mitoses. These neoplastic cells were positive for cytokeratin 19, but staining was weaker than normal ducts in the same livers (not shown). Apoptosis, as judged by terminal dUTP nick-end labeling staining, was infrequent in these ducts (not shown), but single cell necrosis was extensive. At 56 weeks, there were small foci of hepatocellular dysplasia consisting of smaller than normal basophilic hepatocytes with increased nuclear-cytoplasmic ratio maintaining a plate-like architecture.

ALT Activity

Activity of serum ALT is commonly used as an indicator of hepatocellular injury, and ALT levels are often significantly elevated in WD patients.[24] Given marked age-dependent differences in pathology, we examined whether or not there was a correlation between serum ALT and the extent of pathological changes in the KO livers. The ALT levels in 6-week-old mice were elevated up to 10-fold (507.0 ± 294.0 IU/L in *Atp7b*$^{-/-}$ mice compared to 51.3 ± 21.4 IU/L in the control animals), despite unremarkable liver pathology, and remained equally high at the age of 20 weeks (513.7 ± 108.1 IU/L in KO compared to 71.3 ± 16.3 IU/L in control). Subsequently, the ALT level declined and at the age of 44 weeks became very similar to those in control serum (60.0 ± 11.4 in *Atp7b*$^{-/-}$ mice and 101.3 ± 28.4 in control), in agreement with histological findings of restoration of liver parenchyma in large parts of the KO livers.

Cytosol and Nuclei Are the Major Sites of Copper Accumulation

To begin dissecting the biochemical basis of copper-induced changes in the *Atp7b*$^{-/-}$ liver, the subcellular distribution of copper was analyzed after fractionation of liver homogenates. Livers at 6 weeks and 20 weeks were compared, since at these ages copper concentration is similar while the pathology is markedly different. In both cases, accumulated copper was found predominantly (~90%) in the cytosol (Figure 4A). After overnight dialysis of cytosolic fraction using 3000-d cutoff membranes, copper remained in the dialysis tubing (not shown), suggesting that accumulated copper was bound to proteins

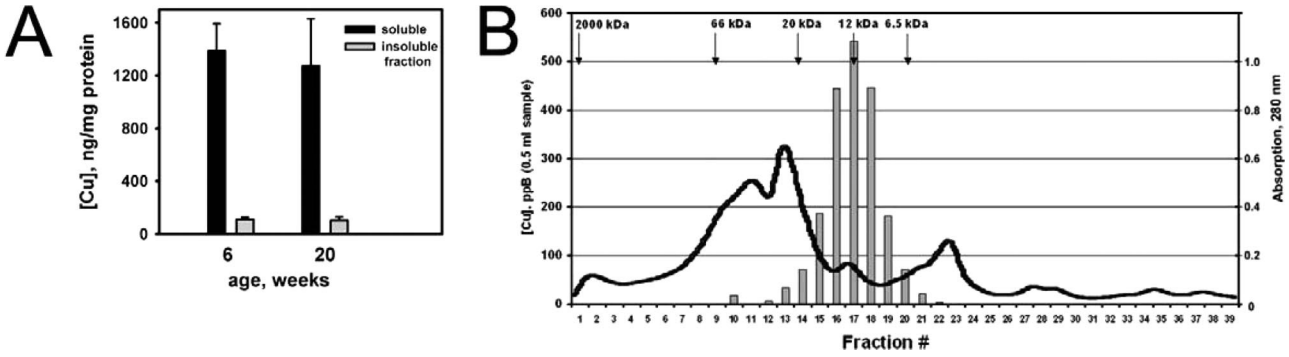

Figure 4. Elevated copper accumulates mostly in the cytosol and binds to small molecular weight protein(s). **A:** Distribution of copper between membrane and soluble fractions isolated from the liver homogenates of *Atp7b*$^{-/-}$ mice at 6 and 20 weeks. **B:** Size-exclusion chromatography of a soluble fraction (6-week-old mice). The **line** indicates a protein elution profile, the **bars** indicate the concentration of copper in the fractions. The **arrows** point to the position of the molecular weight markers.

rather than to low-molecular weight compounds such as glutathione or cysteine. This conclusion was confirmed by the results of size exclusion chromatography (Figure 4B). A single peak of copper in a fraction with the 10- to 20-kd proteins was detected, indicating that copper was bound to a specific protein or subset of proteins.

Copper was also elevated in the nonsoluble fraction from the KO livers (approximately sevenfold; Figure 5A). The nuclei-, mitochondria-, endosome-, and plasma membrane-enriched fractions all showed copper accumulation. However, the degree of copper overload varied for different cell compartments. In the WT samples, copper was almost evenly distributed among membrane fractions with the least copper found in the nuclei-containing fraction (Figure 5B). In contrast, in the KO mice the relative amount of copper in the nuclei-containing fraction was significantly increased, constituting ~30% of total membrane-bound copper (Figure 5B). Proportionally less copper was found in the 125,000 × *g* pellet of KO sample enriched in plasma membranes. The pattern of copper distribution between different membrane fractions was similar for the 6-week-old and 20-week-old livers (Figure 5B).

Nuclear Copper Accumulation Is Associated with the Changes in the Structure and Function of Nuclei

Differential centrifugation generates fractions enriched in certain cell compartments but does not yield pure organelles. Therefore, to verify our conclusion about accumulation of copper in the KO nuclei, we purified nuclear fractions from the control and age-matched KO livers using a sucrose gradient[25] and measured their copper content. The purity of the nuclei was confirmed using organelle markers (Figure 6A). In parallel, livers were used for histology staining to characterize nuclear morphology. These experiments demonstrated an 11- to 12-fold increase in copper concentration in the KO nuclei (Figure 6B), which was associated with marked increase in nuclear size and appearance of prominent nucleoli (Figure 6C).

To characterize the effect of copper on nuclei in more detail we examined whether copper accumulation affects nuclear function. This was evaluated by immunodetection of

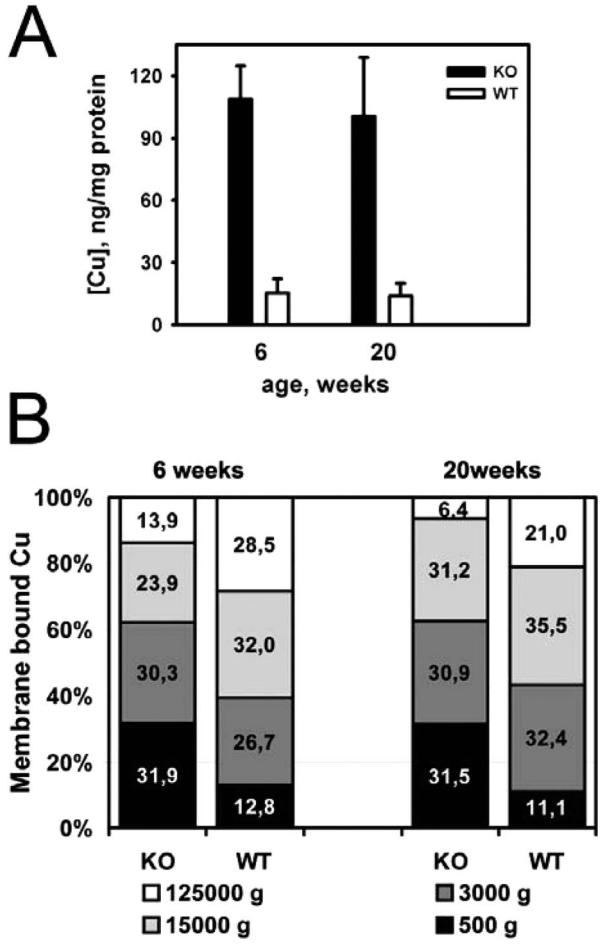

Figure 5. Distribution of copper in subcellular fractions of control (WT) and *Atp7b*$^{-/-}$ (KO) hepatocytes. **A:** Copper concentration in the total membrane fraction from *Atp7b*$^{-/-}$ (**black bars**) and WT (**white bars**) livers at 6 and 20 weeks. **B:** Relative copper distribution in subcellular fractions enriched in nuclei (500 g), mitochondria (3000 g), endoplasmic reticulum, Golgi, lysosome (15,000 g), plasma membranes (125,000 g). The total amount of copper in fractions was taken as 100%.

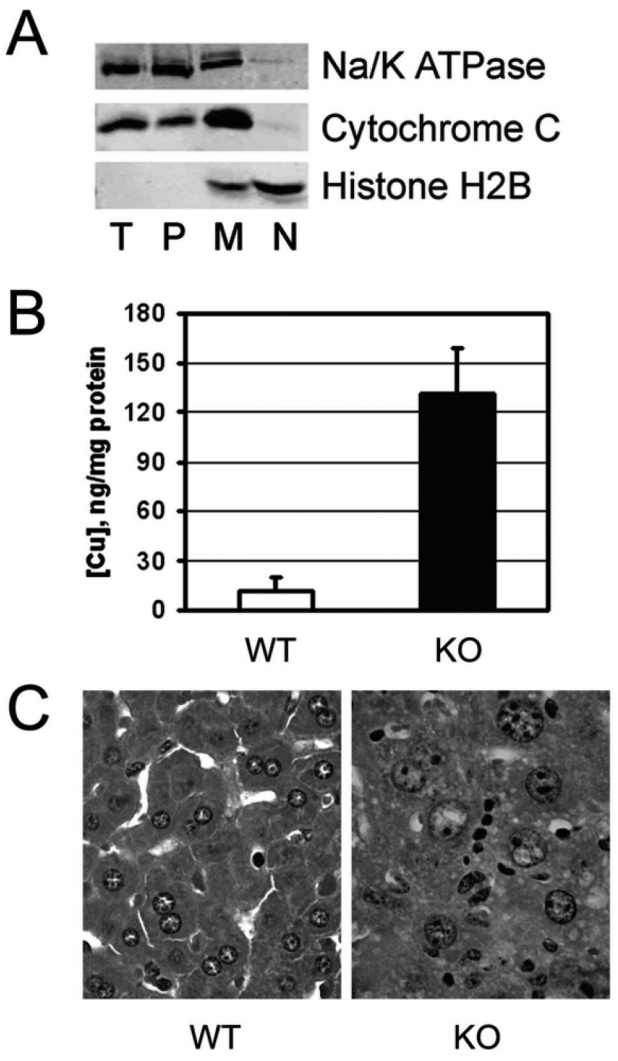

Figure 6. Accumulation of copper in the nuclei is associated with early changes in nuclear structure and function. **A:** Analysis of the purity of nuclear fraction using organelle markers. T, total homogenate; P, postnuclear supernatant; M, crude mitochondria; N, nuclei; Na/K ATPase α 1, marker for plasma membrane; cytochrome *c*, marker for mitochondria; histone H2B, marker for nuclei. **B:** Copper concentration in the purified nuclear fractions. **C:** H&E staining of liver sections from control and *Atp7b*$^{-/-}$ mice. All results are for 6-week-old animals. Original magnifications, ×600.

a nuclear nonhistone protein Ki-67. Immunostaining of Ki-67 in tissues is strongly associated with cell proliferation and increased DNA synthesis.[26] Immunohistochemistry using antibody Mib-1, which can detect Ki-67 in paraffin-embedded tissues,[27] revealed significant Ki-67 staining in *Atp7b*$^{-/-}$ hepatocytes at all ages. Importantly, the staining was observed at the early stages of copper accumulation in the nucleus (at 6 weeks) before appearance of noticeable histopathological alterations (Figure 7A).

We then examined whether restoration of normal parenchyma concurrent with neoplastic transformation of the ducts (see Figure 3F) correlated with changes in DNA synthesis. At 12 weeks, frequent Ki-67 nuclear staining was detected in hepatocytes (Figure 7B), while there were very rare stained nuclei in the normal-appearing portions of the *Atp7b*$^{-/-}$ livers at 44 or 56 weeks (Figure 7C). As described above, at these later stages the *Atp7b*$^{-/-}$ livers also contain multiple foci of cholangitis with foci of neoplastic transformation; in these regions, the Ki-67 staining was very prominent in both the proliferating ducts and nearby hepatocytes (Figure 7D). Interestingly, the increase in DNA synthesis showed a gradient effect depending on proximity to the region of proliferation. In the regions away from the proliferating bile ducts, the Ki-67 staining was minimal (Figure 7E), whereas in the vicinity of the expanding ductal neoplasms the hepatocytes showed distinct threefold to fourfold increase in DNA synthesis (Figure 7F).

Discussion

The Atp7b$^{-/-}$ *Mouse Is a Valuable Model for Analysis of Copper-Induced Pathology in Liver*

Availability of appropriate animal models is an important step toward understanding and effective treatment of WD. To facilitate development of such models, we have characterized *Atp7b*$^{-/-}$ mice, genetically engineered by targeted inactivation of the WD gene. We show that the key manifestations of WD are preserved in these animals. The *Atp7b*$^{-/-}$ mice accumulate copper in the liver, show lack of copper incorporation into ceruloplasmin, marked decrease of oxidase activity in plasma, and elevated copper in urine. (At variance with humans, the mouse apo-ceruloplasmin appears to be more resistant to proteolytic degradation than human protein, as evidenced by the presence of significant amounts of total ceruloplasmin in all *Atp7b*$^{-/-}$ sera). The *Atp7b*$^{-/-}$ mice show dramatic morphological changes in the liver, which progress from mild necrosis and inflammation to a widespread hepatocellular injury and culminates with liver regeneration and changes in the bile duct morphology consistent with cholangiocarcinoma. Altogether, the *Atp7b*$^{-/-}$ mice represent a very useful and interesting model for analysis of copper toxicity in the liver. It is particularly important that marked morphological and biochemical changes, observed in these animals, can be directly linked to inactivation of a single gene, *Atp7b*.

With this in mind, it is interesting to compare the *Atp7b*$^{-/-}$ phenotype with the phenotype of LEC rats and *tx* mice (the *tx*^{j} mice have not been characterized in detail). There are clear similarities, including age-dependent changes in copper concentration in the liver, delay in development of pathological changes compared to the rate of copper accumulation, and marked changes in nuclear morphology. There are also significant differences. For example, LEC rats were reported to develop hepatocellular carcinoma, while this tumor has not been observed in the *Atp7b*$^{-/-}$ mice. Variation in frequency of hepatocellular carcinoma between LEC rat lineages suggests that in rats, gene(s) other than *Atp7b* may facilitate development of this tumor.[14] Interestingly, both lineages of LEC rats display cholangiofibrosis, a condition preceding development of cholangiocarcinoma, which we consistently detect in *Atp7b*$^{-/-}$ mice (see below for details).

There are also clear differences between *Atp7b*$^{-/-}$ mice and *tx* mice in two respects. The *tx* mice were

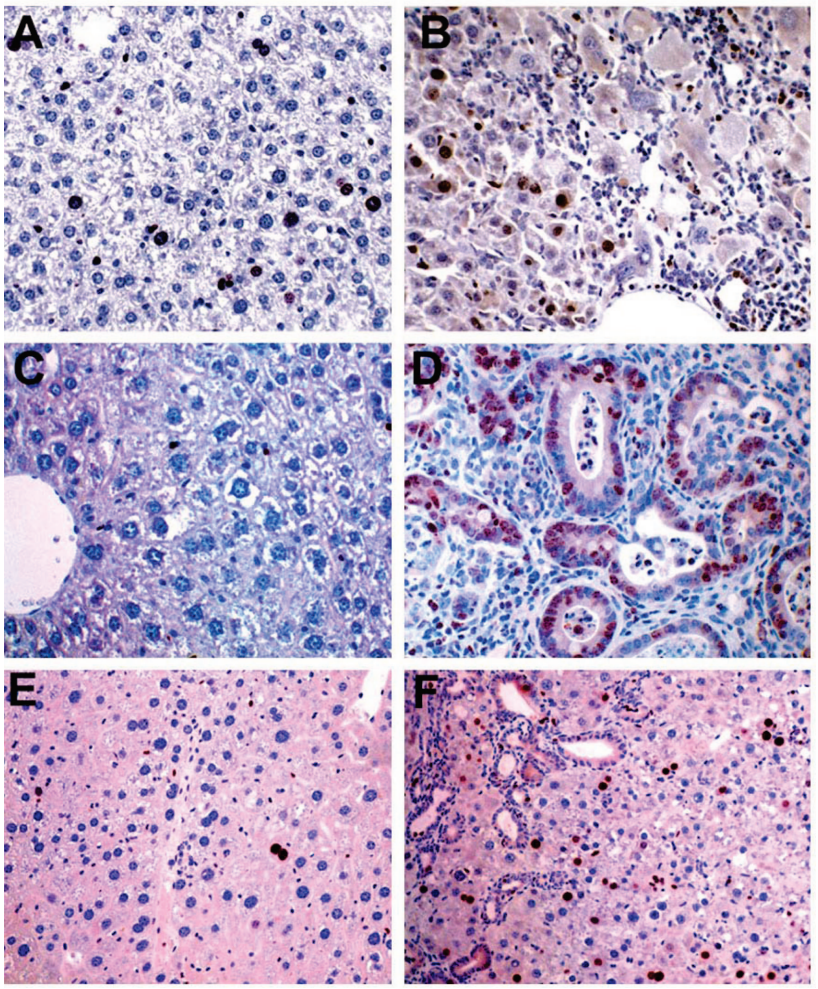

Figure 7. Detection of proliferation marker Ki-67 using immunostaining with Mib1 antibody in the *Atp7b*$^{-/-}$ livers at different stages of the disease. **A:** Six weeks: increased hepatocellular DNA synthesis (black nuclear staining) before detectable hepatocellular injury. **B:** Twelve weeks: many positive hepatocytes at time of maximal injury. **C:** Forty-four weeks: normal-appearing hepatocytes with minimal DNA synthesis. **D:** Forty-four weeks: the proliferating bile duct epithelium is strongly positive. **E:** Fifty-six weeks: minimal hepatocyte staining distant from the cholangitis. **F:** Fifty-six weeks: increased DNA synthesis in the vicinity of the proliferating bile ducts. Original magnifications, ×200.

reported to have severe neurological phenotype and to die at the age of 2 weeks unless nursed by normal dams.[10] In contrast, *Atp7b*$^{-/-}$ mice display such symptoms infrequently (our data), either due to difference in the background strains or presence of additional mutations in the *tx* mice. In contrast to neurological symptoms, the liver phenotype is milder in the *tx* mice compared to *Atp7b*$^{-/-}$ mice and LEC rats. Although inflammation and necrosis are reported, liver pathology develops later compared to *Atp7b*$^{-/-}$ mice (or rats), and changes resembling cholangiocarcinoma or hepatocellular carcinoma are not observed. These differences in phenotypes are likely due to presence in the *tx* liver of a mutant Atp7b protein, which may have residual copper transport activity (no Atp7b protein is produced in either *Atp7b*$^{-/-}$ mice or LEC rats). In fact, recent studies by Voskoboinik and colleagues[28] demonstrate that although the *tx* mutant (Met1386Val substitution in Atp7b) has a markedly decreased copper-translocating activity in the *in vitro* vesicle assay, the expression of mutant Atp7b in cultured cells increases cell resistance to elevated copper indicating that the mutant Atp7b retains some copper transport activity. The availability of two mouse models with partial and complete inactivation of Atp7b (the *tx* mice and *Atp7b*$^{-/-}$ mice, respectively) seems particularly valuable. Numerous WD-causing mutations have been identified in patients; the effect of these mutations on ATP7B intracellular localization and function vary significantly.[29,30] Therefore, two mouse models with different degrees of Atp7b inactivation will help to better dissect the phenotypic diversity, which is characteristic of WD.

Time-Dependent Changes in Copper Concentration

It is notable that with age copper levels decline in both control and *Atp7b*$^{-/-}$ animals (this report and Buiakova et al[16]). Similar age-dependent decrease in hepatic copper was reported in copper overloaded rats[31] and in *tx* mice.[8] Since the expression of *Atp7b* in the WT liver

decreases significantly with age,[32] the observed decline in copper concentration is likely due to age-dependent up-regulation of copper-handling mechanisms independent of Atp7b. The molecular nature of such mechanisms is currently unknown. However, the involvement of the ABC-type transporter MRP2 in the export of copper under conditions of metal overload makes MRP2 an interesting candidate for this role.[33]

Accumulated Copper Induces Distinct Pathological Changes in the Liver

The morphological changes in the *Atp7b*$^{-/-}$ livers are also age-dependent and striking, particularly in older animals. We observed a frequent occurrence of cholangiocarcinoma after earlier hepatocyte dysplasia and bile duct proliferation. The dysplastic changes in the duct epithelium are very severe and consistent with neoplastic transformation, although we did not find any metastases to prove the point. To our knowledge, this is the first description of a mouse model for this tumor. (Heretofore animal models of cholangiocarcinoma have been limited to the Syrian hamster with chemically inducible tumors[34–36].) Interestingly, although tumors are rare in WD, cholangiocarcinomas have been described in several case reports[37–41] as well as in a recent retrospective study of 363 WD patients,[42] suggesting higher frequency of malignancies (cholangio- and hepatocellular carcinomas) in patients with WD than in the control population.

The ductal pathology in the older *Atp7b*$^{-/-}$ mice closely resembles the cholangiofibrosis described and depicted by Schilsky[14] and colleagues in the LEC rat. Although cholangiocarcinomas were not observed in the rats, the authors mentioned the presence of apparent bile duct adenomas and acknowledge the potential for malignant transformation. Altogether, the occurrence of hepatomas in LEC rats and our observation of spontaneous development of cholangiocarcinoma in most *Atp7b*$^{-/-}$ mice indicate that prolonged copper accumulation is associated with increased susceptibility to cancer. The availability of animal models for study copper-induced tumorigenesis has important implications for understanding and treatment of hepatic malignancies.

The restoration of major portions of the *Atp7b*$^{-/-}$ liver after prolonged exposure to elevated copper is another striking observation. Between 20 weeks, when virtually every hepatocyte was injured, and 28 weeks, when the first examples of completely normal architecture and cytology were observed, the liver's remarkable capacity for regeneration was apparent. This phenomenon is unlikely due to spontaneous reversal of the *Atp7b*$^{-/-}$ mutation because the large portion of the *Atp7b* gene-coding region corresponding to exon 2 has been removed in these animals and the neomycin cassette was inserted.[16] We cannot, however, exclude the possibility of an induced splicing event, which would generate a shorter Atp7b mRNA and truncated but functional protein. The experiments testing this hypothesis are currently underway in our laboratory. Alternatively, liver recovery could be due to induced expression of Atp7a, another copper-transporting ATPase, that normally is expressed in embryonic liver.[43] We examined this latter possibility by hybridizing total mRNA extracted from control and *Atp7b*$^{-/-}$ liver with Affymetrix oligonucleotide arrays (see experimental procedures). Although a number of genes showed changed levels of expression, elevation of the Atp7a message was not observed (data not shown) arguing against significant Atp7a involvement in liver recovery.

Nuclear Involvement in the Initial Response to Copper Accumulation

Our results indicate that copper accumulation in nuclei has marked effect on nuclear morphology and function. Previously, elevated copper was detected in hepatic nuclei of WD patients[44] and copper-overloaded sheep,[45] rats,[31] and *tx* mice,[46] indicating that nuclear copper accumulation is a species-independent phenomenon. Increase of nuclear copper in the KO animals is associated with appearance of Ki-67 immunostaining, pointing to increased DNA synthesis. It seems highly significant that both marked increase in nuclear size and appearance of the proliferation marker are observed at the very early stage of copper overload, before development of significant pathological changes. This observation suggests that nucleus is an important and perhaps initial target of copper toxicity and gives support to the hypothesis that WD pathology occurs as a consequence of nuclear disorganization.[31,47]

We do not exclude the role of other organelles in cell response to elevated copper. In fact, our studies demonstrate that copper accumulates in several cell compartments and has a distinct effect on mitochondria morphology, including changes in mitochondria shape and appearance of high-density deposits, just as in the human WD liver. At the same time, the nuclear response to copper accumulation and/or to WD progression may be underappreciated. Not only are there significant changes in DNA synthesis before development of pathological changes (see above), but there is a strong correlation between the number of hepatocytes synthesizing DNA and spatial proximity of hepatocytes to the foci of inflammation and neoplasia. Further studies will determine whether or not the observed gradient in nuclear activity is associated with the gradually changing levels of intracellular copper in corresponding regions or if more complex mechanisms are at play.

In summary, the *Atp7b*$^{-/-}$ mice represent a valuable model for analysis of consequences of copper accumulation in the liver. Several important phenotypic characteristics of the *Atp7b*$^{-/-}$ mice resemble the WD phenotype, encouraging utilization of these animals for dissecting the WD pathology. The early involvement of nuclei, the development of cholangiocarcinoma, and remarkable regeneration of liver after prolonged exposure to copper illustrate a marked complexity of copper biology and suggest important changes in the hepatocellular genetic programs triggered by elevated copper.

Acknowledgments

We thank Dr. Whittaker (Oregon Graduate Institute School of Science and Engineering) for help with atomic absorption experiments; Tina Purnat (Oregon Health & Science University) for assistance with manuscript preparation; Carry Brady (Oregon Health and Science University) for help with histology studies; Angela Major for morphological studies performed in a Core Laboratory (supported by the National Institutes of Health grant P30 DK 56338) and James Barrish for electron microscopy (both at Texas Children's Hospital); and Dr. Hans-Juergen Kuehn (University Leipzig, Leipzig, Germany) and Dr. Uta Merle (University Heidelberg, Heidelberg, Germany) for providing valuable help with the measurements of ceruloplasmin oxidase activity.

References

1. Pena MM, Lee J, Thiele DJ: A delicate balance: homeostatic control of copper uptake and distribution. J Nutr 1999, 129:1251–1260
2. Mercer JF, Llanos RM: Molecular and cellular aspects of copper transport in developing mammals. J Nutr 2003, 133:1481S–1484S
3. Harris ZL, Gitlin JD: Genetic and molecular basis for copper toxicity. Am J Clin Nutr 1996, 63:836S–841S
4. Waggoner DJ, Bartnikas TB, Gitlin JD: The role of copper in neurodegenerative disease. Neurobiol Dis 1999, 6:221–230
5. Loudianos G, Gitlin JD: Wilson's disease. Semin Liver Dis 2000, 20:353–364
6. Riordan SM, Williams R: The Wilson's disease gene and phenotypic diversity. J Hepatol 2001, 34:165–171
7. Ferenci P, Caca K, Loudianos G, Mieli-Vergani G, Tanner S, Sternlieb I, Schilsky M, Cox D, Berr F: Diagnosis and phenotypic classification of Wilson disease. Liver Int 2003, 23:139–142
8. Biempica L, Rauch H, Quintana N, Sternlieb I: Morphologic and chemical studies on a murine mutation (toxic milk mice) resulting in hepatic copper toxicosis. Lab Invest 1988, 59:500–508
9. Coronado V, Nanji M, Cox DW: The Jackson toxic milk mouse as a model for copper loading. Mamm Genome 2001, 12:793–795
10. Rauch H: Toxic milk, a new mutation affecting cooper metabolism in the mouse. J Hered 1983, 74:141–144
11. Theophilos MB, Cox DW, Mercer JF: The toxic milk mouse is a murine model of Wilson disease. Hum Mol Genet 1996, 5:1619–1624
12. Wu J, Forbes JR, Chen HS, Cox DW: The LEC rat has a deletion in the copper transporting ATPase gene homologous to the Wilson disease gene. Nat Genet 1994, 7:541–545
13. Mori M, Hattori A, Sawaki M, Tsuzuki N, Sawada N, Oyamada M, Sugawara N, Enomoto K: The LEC rat: a model for human hepatitis, liver cancer, and much more. Am J Pathol 1994, 144:200–204
14. Schilsky ML, Quintana N, Volenberg I, Kabishcher V, Sternlieb I: Spontaneous cholangiofibrosis in Long-Evans Cinnamon rats: a rodent model for Wilson's disease. Lab Anim Sci 1998, 48:156–161
15. Terada K, Sugiyama T: The Long-Evans Cinnamon rat: an animal model for Wilson's disease. Pediatr Int 1999, 41:414–418
16. Buiakova OI, Xu J, Lutsenko S, Zeitlin S, Das K, Das S, Ross BM, Mekios C, Scheinberg IH, Gilliam TC: Null mutation of the murine ATP7B (Wilson disease) gene results in intracellular copper accumulation and late-onset hepatic nodular transformation. Hum Mol Genet 1999, 8:1665–1671
17. Lowry OJ, Rosebrough NJ, Farr AL, Randall RJ: Protein measurement with the Folin phenol reagent. J Biol Chem 1951, 193:265–275
18. Fleischer S, Kervina M: Subcellular fractionation of rat liver. Methods Enzymol 1974, 31:6–41
19. Packer NH, Pawlak A, Kett WC, Gooley AA, Redmond JW, Williams KL: Proteome analysis of glycoforms: a review of strategies for the microcharacterisation of glycoproteins separated by two-dimensional polyacrylamide gel electrophoresis. Electrophoresis 1997, 18:452–460
20. Ravin HA: An improved colorimetric enzymatic assay of ceruloplasmin. J Lab Clin Med 1961, 58:161–168
21. Schosinsky KH, Lehmann HP, Beeler MF: Automated determination of serum ceruloplasmin activity with o-dianisidine dihydrochloride as substrate. Clin Chem 1975, 21:757–759
22. Hirano K, Ogihara T, Ogihara H, Hiroi M, Hasegawa M, Tamai H: Identification of apo- and holo-forms of ceruloplasmin in patients with Wilson's disease using native polyacrylamide gel electrophoresis. Clin Biochem 2005, 38:9–12
23. Terada K, Nakako T, Yang XL, Iida M, Aiba N, Minamiya Y, Nakai M, Sakaki T, Miura N, Sugiyama T: Restoration of holoceruloplasmin synthesis in LEC rat after infusion of recombinant adenovirus bearing WND cDNA. J Biol Chem 1998, 273:1815–1820
24. Iorio R, D'Ambrosi M, Marcellini M, Barbera C, Maggiore G, Zancan L, Giacchino R, Vajro P, Marazzi MG, Francavilla R, Michielutti F, Resti M, Frediani T, Pastore M, Mazzarella G, Fusco G, Cirillo F: Serum transaminases in children with Wilson's disease. J Pediatr Gastroenterol Nutr 2004, 39:331–336
25. Fleischer S, Kervina M: Subcellular Fractionation of Rat Liver. In: Biomembranes. Edited by Packer L, Fleischer S. San Diego, Academic Press, 1997, pp 7–41
26. Duchrow M, Schmidt MH, Zingler M, Anemuller S, Bruch HP, Broll R: Suppression of cell division by pKi-67 antisense-RNA and recombinant protein. Cell Physiol Biochem 2001, 11:331–338
27. McCormick D, Chong H, Hobbs C, Datta C, Hall PA: Detection of the Ki-67 antigen in fixed and wax-embedded sections with the monoclonal antibody MIB1. Histopathology 1993, 22:355–360
28. Voskoboinik I, La Fontaine S, Mercer JF, Camakaris J: Functional studies on the Wilson copper P-type ATPase and toxic milk mouse mutant. Biochem Biophys Res Commun 2001, 281:966–970
29. Huster D, Hoppert M, Lutsenko S, Zinke J, Lehmann C, Mossner J, Berr F, Caca K: Defective cellular localization of mutant ATP7B in Wilson's disease patients and hepatoma cell lines. Gastroenterology 2003, 124:335–345
30. Morgan CT, Tsivkovskii R, Kosinsky YA, Efremov RG, Lutsenko S: The distinct functional properties of the nucleotide-binding domain of ATP7B, the human copper-transporting ATPase: analysis of the Wilson disease mutations E1064A, H1069Q, R1151H, and C1104F. J Biol Chem 2004, 279:36363–36371
31. Haywood S, Loughran M, Batt RM: Copper toxicosis and tolerance in the rat. III. Intracellular localization of copper in the liver and kidney. Exp Mol Pathol 1985, 43:209–219
32. Schaefer M, Hopkins RG, Failla ML, Gitlin JD: Hepatocyte-specific localization and copper-dependent trafficking of the Wilson's disease protein in the liver. Am J Physiol 1999, 276:G639–G646
33. Dijkstra M, Kuipers F, van den Berg GJ, Havinga R, Vonk RJ: Differences in hepatic processing of dietary and intravenously administered copper in rats. Hepatology 1997, 26:962–966
34. Cheifetz RE, Davis NL, Owen DA: An animal model of benign bile-duct stricture, sclerosing cholangitis and cholangiocarcinoma and the role of epidermal growth factor receptor in ductal proliferation. Can J Surg 1996, 39:193–197
35. Thamavit W, Pairojkul C, Tiwawech D, Itoh M, Shirai T, Ito N: Promotion of cholangiocarcinogenesis in the hamster liver by bile duct ligation after dimethylnitrosamine initiation. Carcinogenesis 1993, 14:2415–2417
36. Imray CH, Newbold KM, Davis A, Lavelle-Jones M, Neoptolemos JP: Induction of cholangiocarcinoma in the Golden Syrian hamster using methylazoxymethyl acetate. Eur J Surg Oncol 1992, 18:373–378
37. Kosminkova EN, Generalova S, Ponomarev AB: The development of diffuse cholangiocarcinoma in a female patient with long-term undiagnosed Wilson's disease. Ter Arkh 1995, 67:85–87
38. Wilkinson ML, Portmann B, Williams R: Wilson's disease and hepatocellular carcinoma: possible protective role of copper. Gut 1983, 24:767–771
39. Polio J, Enriquez RE, Chow A, Wood WM, Atterbury CE: Hepatocellular carcinoma in Wilson's disease. Case report and review of the literature. J Clin Gastroenterol 1989, 11:220–224
40. Cheng WS, Govindarajan S, Redeker AG: Hepatocellular carcinoma in a case of Wilson's disease. Liver 1992, 12:42–45
41. Ponomarev AB, Kosminkova EN, Generalova S: Diffuse cholangiocar-

inoma in the context of multilobular liver cirrhosis as a manifestation of Wilson-Konovalov disease. Arkh Patol 1994, 56:74–77
42. Walshe JM, Waldenstrom E, Sams V, Nordlinder H, Westermark K: Abdominal malignancies in patients with Wilson's disease. QJM 2003, 96:657–662
43. Kuo YM, Gitschier J, Packman S: Developmental expression of the mouse mottled and toxic milk genes suggests distinct functions for the Menkes and Wilson disease copper transporters. Hum Mol Genet 1997, 6:1043–1049
44. Yano M, Sakamoto N, Takikawa T, Hayashi H: Intrahepatocellular localization of copper in Wilson's disease. Nagoya J Med Sci 1993, 55:131–137
45. Gooneratne SR, Howell JM, Gawthorne J: Intracellular distribution of copper in the liver of normal and copper loaded sheep. Res Vet Sci 1979, 27:30–37
46. Howell JM, Mercer JF: The pathology and trace element status of the toxic milk mutant mouse. J Comp Pathol 1994, 110:37–47
47. Deng DX, Ono S, Koropatnick J, Cherian MG: Metallothionein and apoptosis in the toxic milk mutant mouse. Lab Invest 1998, 78:175–183